A computational convection analysis of $SiO_2/water$ and $MOS_2 - SiO_2/water$ based fluidic system in inverted cone

Iftikhar Ahmad[a], Syed Ibrar Hussain[b,*], Muhammad Zulfiqar Umer[a], Muhammad Asif Zahoor Raja[c]

[a]*Department of Mathematics, University of Gujrat, 50700 Gujrat, Pakistan*
[b]*Department of Mathematics and Computer Science, University of Palermo, Via Archirafi 34, 90123 Palermo, Italy*
[c]*Future Technology Research Center, National Yunlin University of Science and Technology, 123 University Road, Section 3, Douliou, Yunlin 64002, Taiwan*

Abstract

A complete shape factor investigation of water-based mixture type hybrid nano-fluid in a permeable boundary with the impact of magnetic field, thick dissemination, and warm radiation is presented in this article. A computational convection analysis of an inverted semi vertical cone with a porous surface in the form of $SiO_2/water$ nano-fluid and $MOS_2 - SiO_2/water$ hybrid nano-fluid transport is developed. The system of differential equations is presented and resolved numerically by the Lobatto IIIA method. The temperature distributions and fluid velocity are studied along with the coefficient of skin friction and the nusselt number, taking into account the form of distinct nano-particles. The flow problem's results are approximated by using several embedding variables. Tables and graphs are constructed for a variety of scenarios including maximum residual error, mesh points, and nusselt numbers. We conclude that boundary film thickness reduces and the fluid flow is resisted by magnetic field presence. Fluid flow slows down as λ increases, and this reduction is more evident in nanofluids than in hybrid nanofluids. With an increment in S, velocity drops. A detailed analysis of the proposed ordinary differential equations, boundary conditions, and numerical data of skin friction is given both in tabular and graphical forms. Additionally, it is observed that the fluid flow slows down more for the hybrid nanofluid than for the $SiO2/water$ nanofluid. Additionally, it is clear that the temperature increase for the $SiO2/water$ nanofluid is substantially greater. The authors deduce that the existence of a magnetic field resists fluid flow for hybrid nanofluid forms and decreases the thickness of the viscous boundary layer.

Keywords: Porous medium (PM); Shape factors; Isothermal cone; Lobatto IIIA approach; Hybrid nano fluid (HNF); Nano fluid (NF).

Nomenclature:
μ_{nf}, μ_{hnf}: Viscosity of NF and HNF
ρ_{nf}, ρ_{hnf} : Density of NF and HNF
$\frac{k_{nf}}{k_f}$, $\frac{k_{hnf}}{k_f}$: Thermal conductivity of NF and HNF
$\left(\rho c_p\right)_{nf}, \left(\rho c_p\right)_{hnf}$: Heat capacity of NF and HNF
v_w: Suction velocity
q_r: Radiative heat flux
σ^{**}: Stefan Boltzmann constant
k^{**}: Coefficient of mean proportion
ψ: Stream function
Gr_x: Rayleigh number
Pr: Prandtl number
Ec: Eckert number
M: Hartmann number
N: Radiation parameter
Nu: Nusselt number
C_f: Skin friction coefficient
τ_w: Shear stress
Nu_x: Local Nusselt number
λ: Power law index
T_w: Wall temperature of inverted cone

1. Introduction

The **base fluids** with low viscosity and thermal conductivity, such as glycol, water, and alcohol cannot be employed solely in many applications of science and technology because of their structure and limited properties. Due to this vulnerability, a new class of fluid called NFs has been introduced. Such NFs are frequently utilized for macroscopic cooling because of the crucial characteristics of heat transport. The single-phase modeling approach of NFs is especially important for lubricant refining, coolants, and applications in daily life including portable computer systems, air conditioners, coolers, and nanostructures. In the manufacturing industry, solar thermal collectors are recognized as a highly straightforward and environmentally friendly way to convert UV irradiation to heat energy. In such collectors, various fluids such as glycol and water are used to improvise their performance and power. Recently, numerically and experimentally, several researchers have researched the use of NFs in many kinds of solar collectors [1], [2], [3]. Many researchers

*Corresponding author
Email addresses: dr.iftikhar@uog.edu.pk (Iftikhar Ahmad), syedibrar.hussain@unipa.it (Syed Ibrar Hussain), 21016109-005@uog.edu.pk (Muhammad Zulfiqar Umer), rajamaz@yuntech.edu.tw (Muhammad Asif Zahoor Raja)

and engineers have recently shown a strong interest in the subject of two-dimensional axially symmetric fluid motion inside a quasi-inverted cone. These flows offer important applications in a variety of engineering and manufacturing processes, such as the design of sustainable power plant equipment, gas turbines, propulsion systems for aircraft, spacecraft, missiles,satellites, storage of grains, the disposal of nuclear waste, the spread of chemical contaminants through water-saturated soil, and other processes that involve the movement of moisture through air trapped in fibre insulations [4], [5].

A **hybrid nanofluid** (HNF) covers nano-particles of various sorts. Synergistic results provide the HNF to integrate advantages from component nano-particles but avoid their drawbacks. This feature results in the properties of HNF as compared to mono-particle-based NFs. Because of the minute size of the nano-particles and their very large common surface area, NFs have useful properties such as high-temperature conductivity, durable stability, minimum obstruction in flow passes, and homogeneity [6], [7], [8]. Choi and Eastman developed the idea of NFs for the suspension of ultrafine particulate liquids [9]. Khan and Pop have found the issue of flow over the stretch sheets in their initial work on NF [10]. Gorla and Chamkha examined the problem of NF flow with natural laminar boundary across the horizontal plate of the porous medium (PM) [11]. Gireesha has studied the effects of tiny particles suspended from a stretching layer in such an NF solution [12].

In this research, a complete shape factor investigation of water-based mixture NF in a permeable boundary alongside the impact of transverse attractive field, thick dissemination, and warm radiation is given. This article presents a computational convection analysis of an inverted cone with a porous surface in the form of Sio_2/water NF and $MoS_2 - Sio_2$/water hybrid NF transport. Temperature distributions and NF velocity are studied, along with the coefficient of nusselt number and the skin friction, taking into account the form of distinct nano-particles. The system of differential equations was simplified and numerically resolved using the lobatto IIIA method. The main findings from the present research are that the existence of a magnetic field resists flow for NF and HNF forms and decreases the thickness of the viscous boundary layer.

Table 1: Experimental values for fluidic system

Properties	H_2O	SiO_2	MOS_2
Specific heat, C_p(J/kgK)	4179	730	397.746
Density, $\tilde{\rho}$(kg/m^3)	0.613	1.5	34.5
Thermal conductivity, $\tilde{k}$(W/mk)	997	2650	5060

1.1. ***Literature Review***

Nadeem described the modeling across a linear and significantly stretching layer of such a two-dimensional natural flow assessment of Williamson fluid [13]. Hayat discusses a time-independent magnetohydrodynamics flow solution for Williamson fluid flow through a porous plate. NFs are arranged by dissolving the nano-particles in the base fluid and can considerably improve the heat conduction and get a heat transfer rate resembling that of pure fluids. NFs introduced by Choi have thermal conductivities in magnitudes, more than the conductivities of the base fluids, and with sizes suggestively smaller than 100 nm. The presence of nano-particles upgrades the warmth move execution of the base fluid fundamentally. In

Table 2: Experimental values for nano-fluidic system

Properties	**NF**
Viscosity	$\mu_{nf} = \frac{\mu_f}{(1-\varphi)^{2.5}}$
Density	$\rho_{nf} = \rho_f(1-\varphi) + \varphi(\rho_s)$
Thermal conductivity,	$\frac{k_{nf}}{k_f} = \frac{k_s+(m-1)k_f-\varphi(m-1)(k_f-k_s)}{k_s+(m-1)k_f+(k_f-k_s)}$
Heat Capacity	$(\rho c_p)_{nf} = (\rho c_p)_f(1-\varphi) + \varphi(\rho c_p)_s$

1979, Chiou calculated the laminar convection flow in the cone frustum. It was assumed that the temperature and the heat flux of the wall not changing and then reached a conclusion that the temperature was inversely proportional to the Prandtl number when moving along the wall of frustum [14]. Yih studied heat transfer and mass transfer of heat (convection) over an inverted cone with the porous medium have to change wall temperature and flux [15]. Later, Chamkha analyzed the function of thermal radiation and also measured the effect of the magnetic field, concluding that the dimensionless numbers like Nusselt number and Sherwood number along with skin friction number reduced by increasing the magnitude of the local Nusselt number, local skin-friction coefficients and the local Sherwood number decrease as Hartmann number increases [16]. Moreover, in 2010 nano-particles effect on a convecting layer at the boundary present in a vertical sheet was studied by Kuzentov [17]. They also studied this problem for porous mediums later [18]. Mass and heat transfer experiments of chemical change

Table 3: Experimental values for HNF system

Properties	**Hybrid NF**
Viscosity	$\mu_{hnf} = \frac{\mu_f}{(1-\varphi_1)^{2.5}(1-\varphi_2)^{2.5}}$
Density	$\rho_{hnf} = \rho_f(1-\varphi_2)\left[(1-\varphi_1) + \varphi_1\left(\frac{\rho_{s_1}}{\rho_f}\right)\right] + \varphi_2\rho_{s_2}$
Thermal cond.	$\frac{k_{hnf}}{k_f} = \frac{k_{s_2}+(m-1)k_{bf}-\varphi_2(m-1)(k_{bf}-k_{s_2})}{k_{s_2}+(m-1)k_{bf}+(k_{bf}-k_{s_2})}$
Heat Cap.	$(\rho c_p)_{hnf} = (\rho c_p)_f(1-\varphi_2)\left[(1-\varphi_1) + \varphi_1\left(\frac{(\rho c_p)_{s_1}}{(\rho c_p)_f}\right)\right] + \varphi_2(\rho c_p)_{s_2}$

effect on fluids over a porous and stretching surface have a major role in the industries of chemical engineering. Chamkha obtained the numerical results of the steady boundary layer with stagnation point of the polar fluid flow moving on the stretched surface embedding in the PM in the existence of the effect of Dufour and Soret numbers and the homogeneous chemical reaction [19]. Kasim studied the effect of a chemical reaction and thermal radiation on a time-dependent stretching sheet of magneto-hydrodynamic flow with free convection boundary layer with mass and heat transfer of such a highly conductive fluid [20]. EL-Aziz studied the numerical solution to investigate the effects of the time-dependent chemical reactions on the heat and mass transfer of NF and stagnation point flow on the stretching surface [21]. The authors of this research article have

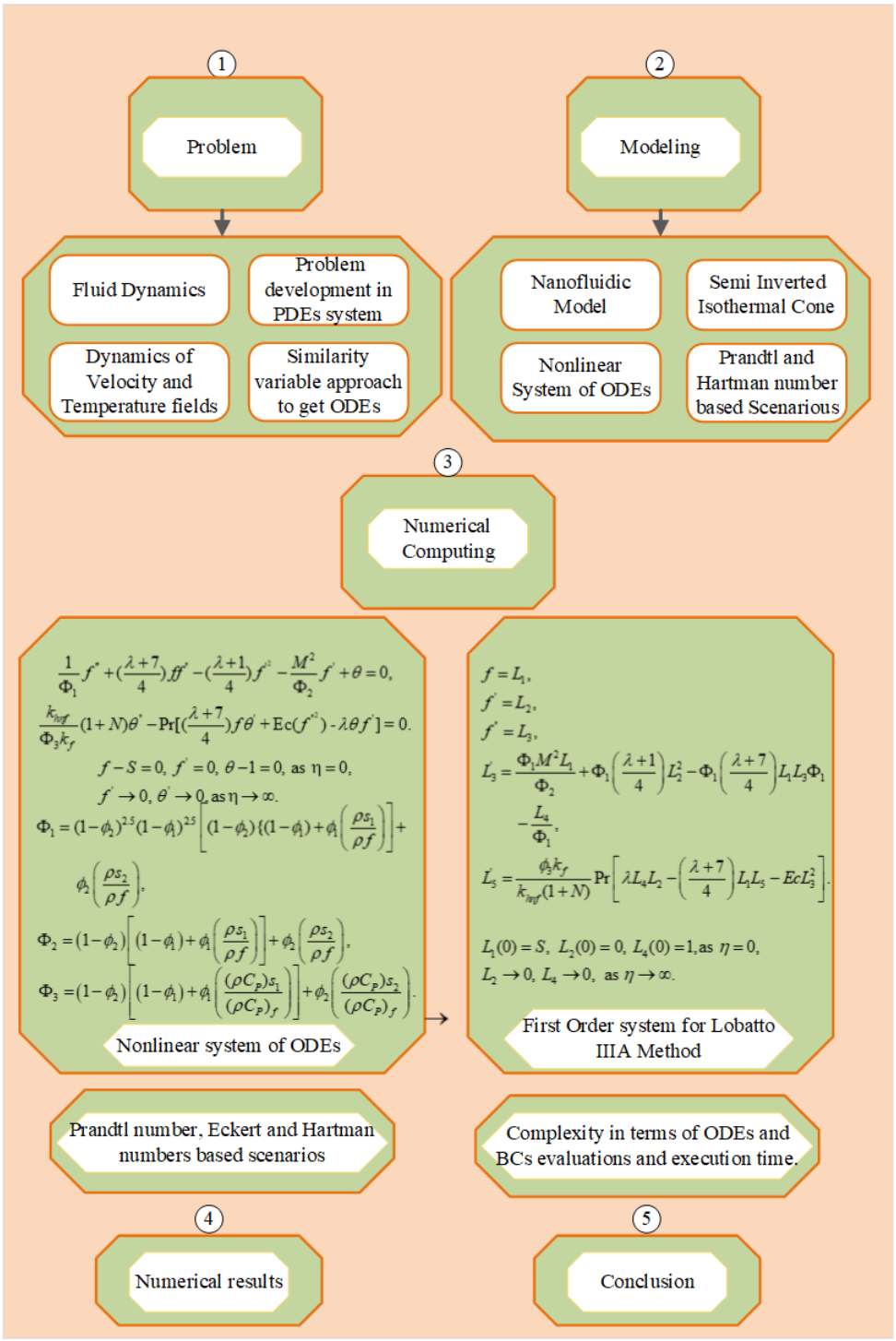

Figure 1: Graphical illustration of numerical methodology

done some previous works in the field of differential equations, especially on non-linear partial differential equations by using a numerical technique to ensure the stability and convergence of the obtained results [22], [23], [24], [25]. A few years ago, Noghrehabadi discussed convection through NF over standing plates pasted in permeable medium surface heat flux in [26]. Water flow, glycol, and ethylene-based NF flow having natural convection through vertical cone on a PM are given in [27]. This research was extended by Ellahi, he found the effects of shape and size of nano-particles on entropy [28]. Namburu calculated copper oxide's viscosity in nano-particles suspended in ethylene glycol and H_2O mixtures. Later, he found a relationship between particle volume viscosity and temperature based on the data. They studied the rheological comportment of NFs [29]. It was observed by Chen that the shear thinning behavior of NFs was dependent on the thickness of particles, viscosity and fluid flow rate [30]. Chan and Dinge studied the behavior of NFs having titanite as constituent nano-particles. They concluded that titanite has very strong thinning properties for NFs and also, they have a huge impact on the concentration and temperature of the medium [31]. Then the results obtained were matched with other results of experiments on various kind of particles, and it showed a very good resemblance with their results [32]. Afshaari and Akbaree examined the nano-particles effects on the viscosity of NFs where it was determined that viscosity increases with the rise of volume fraction of nano-particles [33]. Kaang and Kime discussed natural convection which is a type of heat transfer in which fluids flow does not depend on an outer source. They also discussed some examples related to the research work [34].

1.2. *Lobatto IIIA Method*

Lobatto IIIA method is applied for the numerical investigation of differential equations which are described by the use of approximations to the solution at endpoints. Due to strong stability properties, Lobatto IIIA methods have been considered for boundary value problems (BVP). We use the Lobatto IIIA method for numerical treatment since it is stiffly accurate. In this work, the authors have presented the analysis for the various values of mesh points and real tolerance to check the efficiency, stability, and reliability of proposed technique. In this research work, we analyzed the results of cross diffusion into a porous medium on the skin friction coefficient, mass and heat transfer from cone into a porous medium. A Lobatto IIA method is used to find numerical solutions for energy, concentration, and momentum equations.

Using the Lobatto IIIA method, Nagoor [35] explained numerically the effect of different physical constraints on velocity and temperature fields for Darcy-Forchheimer HNF flow in revolving frames. The above-mentioned experiments in which many researchers presumed different fluids with various nano-particles and observed interesting findings for their thermophysical behavior are the motivation behind this proposed study. There is substantial research being conducted on the numerical approach to the problem of NF flow [36], [37], [38], [39], but relatively few researchers have attempted to solve the problem of hybrid flow of NF using special numerical methods. The present article offers a detailed form study of $MoS_2 - SiO_2/water$ water-dependent HNF inside a semi vertical and inverted cone having porous boundary as well as the impact of the presence of the magnetic field, viscous dissipation including thermal radiation.

1.3. *Highlights*

The following are a few of the important aspects of this research:

- The radiative flow of HNFs $MoS_2 - SiO_2/water$ over a semi-inverted cone with porous boundary effects has been modeled in a novel way, using the power of sufficient similarity transformations, PDEs describing the flow model are converted into a system of ODEs.
- A computational investigation by exploiting the Lobatto IIIA approach is implemented for the dynamical analysis of a hybrid nano-fluidic system passed over a semi-inverted cone with a porous boundary.
- The primary approach of boundary layer approximations is applied to systemize the governing nonlinear PDEs of the nano-fluidic and hybrid nano-fluidic model and these PDEs are converted into ODEs by the competence of similarity variables.
- The implementation of a numerical approach namely Lobatto IIIA technique that relates to the categories of finite difference numerical techniques for examining the nano-fluidic model, is a novel work.
- The graphical illustration of each fluidic parameter on velocity and temperature fields is portrayed along with the numerical computed data of Skin friction coefficient and Nusselt-number for assessment analysis.

1.4. *Organization of the paper*

The rest of the sections of the manuscript are cataloged as follows: Section two describes flow equation modeling, Section three provides numerical results & discussion and Section four summarizes the fluidic system's conclusion and recommendations.

2. Modeling and Simulation of nano-fluidic equations

The development of physical problems involves an isothermic cone with an inverted porous medium in which the flow of an NF is a 2D steady-state and incompressible, is presented. ω is a semi-vertical angle along with the cone. The origin of the cartesian coordinates system is taken from vertex of cone. Moreover, we chose the $x - axis$ and $y - axis$ as parallel and perpendicular to surface of inverted cone, respectively. The physical abstract of proposed model is illustrated in Fig. 2. Considering the existence of viscous properties and the effects of thermal energy, heat transmission is involved on surface of the cone (inverted). Also, we take temperature T as a constant value [4].

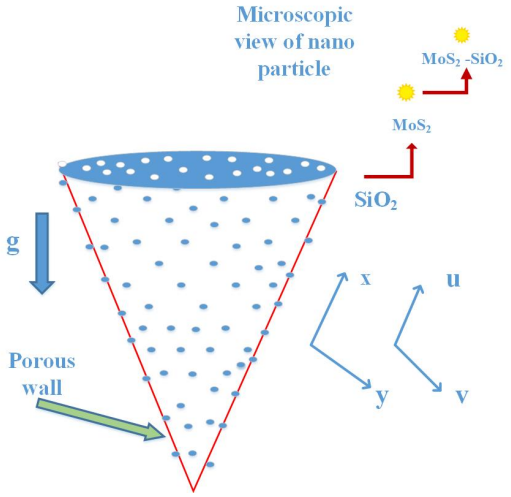

Figure 2: Physical diagram of the nano-fluidic model

The temperature of the wall of an inverted cone is defined as $T_w = ax^{\lambda} + T_\infty$ where a($a > 0$) is constant and T_∞ is temperature distant from the cone surface and its property is $T_\infty > T_\infty$. Also, λ is power index law. Under these assumptions, along with the approximations of boundary layers, the governing equations are determined as follow:

$$\frac{\partial}{\partial x}(ur) + \frac{\partial}{\partial y}(vr) = 0, \tag{1}$$

$$u\frac{\partial u}{\partial x} + v\frac{\partial u}{\partial y} = \frac{1}{\rho_{hnf}}\left[\mu_{hnf}\frac{\partial^2 u}{\partial y^2} + g(\rho\beta)_{hnf}(T - T_\infty) - \sigma^2\beta^2 u\right], \tag{2}$$

$$u\frac{\partial T}{\partial x} + v\frac{\partial T}{\partial y} = \frac{\mu_{hnf}}{\left(\rho c_p\right)_{hnf}}\left[\left(\frac{\partial u}{\partial y}\right)^2 - \frac{1}{\mu_{hnf}}\frac{\partial q_r}{\partial y}\right] + \alpha_{hnf}\frac{\partial^2 T}{\partial y^2}. \tag{3}$$

The attached boundary conditions are:

$$\begin{aligned} u = 0,\ \ v = v_w,\ \ T = T_w = ax^{\lambda} + T_\infty,\ \ \text{on}\ \ y = 0,\ \ x \geqslant 0, \\ u = 0,\ \ T \longrightarrow T_\infty\ \ \text{as}\ \ y \longrightarrow \infty. \end{aligned} \tag{4}$$

where u and v are components of velocity along x and y directions, with thin boundaries $r = x\sin\omega$. The density of the HNF is ρ_{hnf}. The dynamic viscosity of HNF is μ_{hnf}. T is the temperature of HNF and q_r is a flux which depends on the temperature of the body. g is a gravitational acceleration and v_w is a suction velocity on the surface of inverted cone. According to the Rosseland approximation [4], radiative heat flux is defined as:

$$q_r = -\frac{4\sigma^{**}}{3k^{**}}\frac{\partial T^4}{\partial r}. \tag{5}$$

here σ^{**} and k^{**} are the Stefan-Boltzmann constant and coefficient of mean proportion. Also we introduced the stream function Ψ as flows:

$$u = \frac{1}{r}\frac{\partial \Psi}{\partial y} \quad and \quad v = -\frac{1}{r}\frac{\partial \Psi}{\partial x}. \tag{6}$$

Now we introduce the following similarity transformations as:

$$\begin{aligned} u = \tfrac{v_f}{x}f' Gr_x^{\frac{1}{4}},\ \ \eta = \tfrac{x}{y}Gr_x^{\frac{1}{4}},\ \ \theta(\eta) = \tfrac{T_\infty - T}{T_\infty - T}, \\ v = \tfrac{v_f}{x}Gr_x^{\frac{1}{4}}(f - \eta f'),\ \Psi = v_f r Gr_x^{\frac{1}{4}} f(\eta). \end{aligned} \tag{7}$$

where Gr_x is Rayleigh number and mathematically given by:

$$Gr_x = \frac{g(\rho\beta)_{hnf}\cos\omega(T_w - T_\infty)x^3}{v_f^2}. \tag{8}$$

Since Eq. (1) is already satisfied and now we substitute the transformations defined in Eq. (4) into the Eq. (1) to Eq. (3) and we get following coupled ODEs:

$$\frac{1}{\Phi_1}f''' + \left(\frac{\lambda + 7}{4}\right)ff'' - \left(\frac{\lambda + 1}{4}\right)(f')^2 - \frac{M^2 f'}{\Phi_2} + \theta = 0, \tag{9}$$

$$\frac{k_{hnf}}{\Phi_3 k_f}(1 + N)\theta'' + P_r\left[\left(\frac{\lambda + 7}{4}\right)f\theta' + Ec(f'')^2 - \lambda\theta f'\right] = 0. \tag{10}$$

$$\begin{aligned} f - S = 0,\ \ f' = 0,\ \ \theta - 1 = 0,\ \ \text{as}\ \ \eta = 0, \\ f' = 0,\ \ \theta = 0,\ \ \text{as}\ \ \eta = \infty. \end{aligned} \tag{11}$$

The mathematical expressions of Φ_1, Φ_2 and Φ_3 are defined as:

$$\Phi_1 = (1 - \varphi_2)^{2.5}(1 - \varphi_1)^{2.5}\left[(1 - \varphi_2)\left\{(1 - \varphi_1) + \varphi_1\left(\frac{\rho_{s_1}}{\rho_f}\right)\right\}\right] + \varphi_2\left(\frac{\rho_{s_2}}{\rho_f}\right), \tag{12}$$

$$\Phi_2 = (1 - \varphi_2)\left[(1 - \varphi_1) + \varphi_1\left(\frac{\rho_{s_1}}{\rho_f}\right)\right] + \varphi_2\left(\frac{\rho_{s_2}}{\rho_f}\right), \tag{13}$$

$$\Phi_3 = (1 - \varphi_2)\left[(1 - \varphi_1) + \varphi_1\frac{\left(\rho c_p\right)_{s_1}}{\left(\rho c_p\right)_f}\right] + \varphi_2\frac{\left(\rho c_p\right)_{s_2}}{\left(\rho c_p\right)_f}. \tag{14}$$

The mathematical expression of prominence fluidic parameter of interest for proposed nano-fluidic system are defined as:

$$\begin{aligned} M = \tfrac{\sigma_{hnf}B_0^2 x^2}{\mu_f Gr_x^{\frac{1}{2}}},\ \ S = \tfrac{v_w x}{v_f Gr_x^{\frac{1}{2}}},\ \ Ec = \tfrac{\mu_f x^2}{Gr_x^{\frac{1}{2}}}, \\ N = \tfrac{16T_\infty^3 x^2}{3k^{**}k\mu_f\left(c_p\right)_f Gr_x^{\frac{1}{2}}},\ \ Pr = \tfrac{\mu_f\left(c_p\right)_f}{k_f}. \end{aligned} \tag{15}$$

where, Pr represents Prandtl number, Ec is Eckert number, M is Hartman number and N is radiation parameter respectively. Here $f(\eta) = S$ when $\eta = 0$ with $S < 0$ being suction case and $S > 0$ shows injection case. The Nusselt number Nu and skin friction coefficient C_f are defined as:

$$Nu = \frac{q_w}{k_{hnf}(T_w - T_\infty)},\ \ C_f = \frac{\tau_w}{\rho_{hnf}u_w^2}. \tag{16}$$

The expression of shear stress on the surface of the cone is indicated by τ_w and given as:

$$\tau_w = \mu_{hnf}\left(\frac{\partial u}{\partial y}\right),\ \ \text{at}\ \ y = 0. \tag{17}$$

The q_w shows the heat flux from the surface of the cone and defined as:

$$q_w = (q_r)_w - k_{hnf}\left(\frac{\partial T}{\partial y}\right), \quad \text{at } y = 0. \tag{18}$$

After solving from Eq. (16) to Eq. (18), we obtain the dimensionless form of Nusselt number Nu_x and skin-friction $C_f Gr_x^{\frac{1}{4}}$ which are given as:

$$C_f Gr_x^{\frac{1}{4}} = \frac{f''(0)}{(1-\varphi)^{2.5}}, \quad Nu_x = -\left(N + \frac{k_{hnf}}{k_f}\right)\theta'(0). \tag{19}$$

3. Results and discussion

Here, the empirical results of fluidic parameters on fluid velocity and temperature distributions are analyzed graphically. Furthermore, tabular forms are created for relevant physical parameters namely, the Nusselt number and skin friction coefficient for various nano-materials shape factors throughout the conduct of HNF $MoS_2 - SiO_2/water$ and dotted lines will be used to show $SiO_2/water$ NF results, respectively. For this purpose, the coupled nonlinear ordinary differential system of the nano-fluidic model is derived from governing PDEs by the exploitation of the non-dimensional similarity variables approach. The transformed nano-fluidic differential system of ODEs presented in Eq. (9) to Eq. (10) are tackled numerically along with attached boundary conditions Eq. (12) by employing the Lobatto IIIA approach with MATLAB routine 'bvp4c'. Power law λ is analyzed through Fig3. The fluid is shown to decelerate with such addition in λ and this reduction in the fluid flow for NF compared to HNF is more pronounced.

Fig4 shows the effect of a magnetic field parameter M on

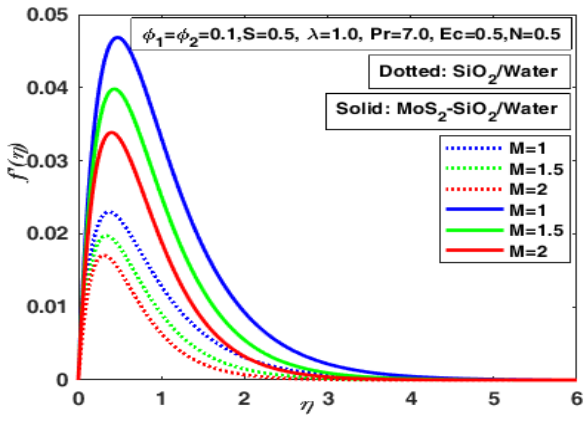

Figure 3: Influence of Power index (λ) on $f'(\eta)$

$f'(\eta)$, so it suffices that the existence of the magnetic field resists fluid flow for NF and HNF. Fig5 is sketched to analyze the influence of N thermal radiation parameter on the velocity profile of NF and HNF, respectively. Here, N relates to the acceleration of flowing fluid and the density of the NF and HNFs at the boundary layer of momentum. Fig6 shows the influence of parameter S on SiO_2/H_2O and $MoS_2 - Sio_2/H_2O$ NFs velocity. It is notable that S presents two cases, if $S > 0$, it presents

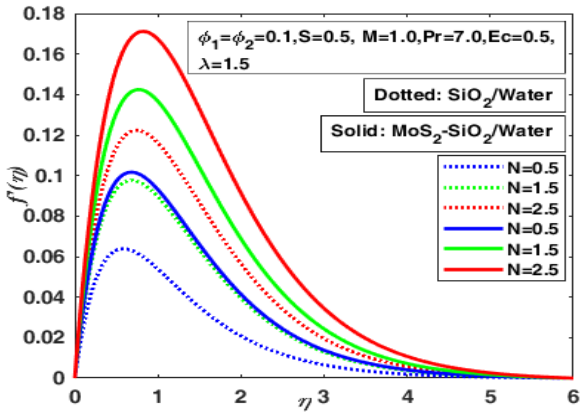

Figure 4: Influence of Hartmann number (M) on $f'(\eta)$

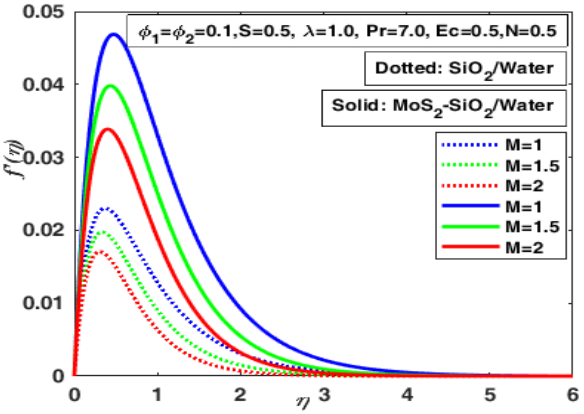

Figure 5: Effect of radiation parameter N on $f'(\eta)$

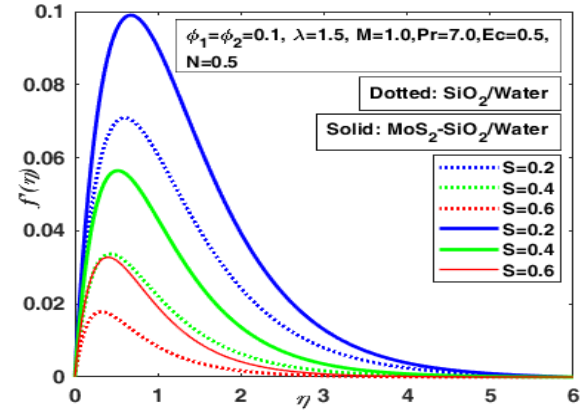

Figure 6: Effect of S on $f'(\eta)$

Table 4: The effect of Mesh points on convergence of SiO_2/H_2O and $MoS_2 - Sio_2/H_2O$

Convergence Limit	Scenarios	SiO_2/H_2O			$MoS_2 - Sio_2/H_2O$		
		Case-1	**Case-2**	**Case-3**	**Case-1**	**Case-2**	**Case-3**
1E-09	**1**	1342	1425	1589	1527	1539	1668
	2	1699	1789	1789	1790	1199	1199
	3	1425	1271	1395	1539	1474	1673
	4	1373	1727	1530	1179	1565	1254
	5	1392	1673	1536	1198	1559	1481
	6	1343	1327	1407	1265	1402	1578
	7	1261	1261	1261	1261	1363	1363
	8	1789	1789	1789	1789	1508	1508
	9	1789	1789	1789	1789	1468	1468
	10	1699	1699	1699	1699	1655	1595
1E-12	**1**	1342	1425	1589	1527	1539	1668
	2	1699	1789	1789	1790	1199	1199
	3	1425	1271	1395	1539	1474	1673
	4	1373	1727	1530	1179	1565	1254
	5	1392	1673	1536	1198	1559	1481
	6	1343	1327	1407	1265	1402	1578
	7	1261	1261	1261	1261	1363	1363
	8	1789	1789	1789	1789	1508	1508
	9	1789	1789	1789	1789	1468	1468
	10	1699	1699	1699	1699	1655	1595

Table 5: The illustration of Residual error analysis of SiO_2/H_2O and $MoS_2 - Sio_2/H_2O$

C L	Scenarios	SiO_2/H_2O			$MoS_2 - SiO_2/H_2O$		
		Case-1	**Case-2**	**Case-3**	**Case-1**	**Case-2**	**Case-3**
1E-09	**1**	3.09E-11	2.68E-11	4.23E-11	1.93E-12	3.11E-12	4.57E-12
	2	2.20E-12	1.83E-12	1.47E-12	1.90E-12	7.57E-12	6.94E-12
	3	2.68E-11	7.88E-11	6.92E-10	3.11E-12	3.53E-12	3.99E-12
	4	6.99E-11	5.97E-12	9.89E-12	4.90E-11	3.00E-12	1.54E-11
	5	3.31E-12	1.54E-12	9.47E-13	7.47E-12	8.61E-13	6.24E-13
	6	2.14E-12	1.52E-11	1.72E-10	2.85E-12	1.29E-12	1.12E-11
	7	2.31E-11	2.31E-11	2.31E-11	2.31E-11	1.97E-11	1.97E-11
	8	1.83E-12	1.83E-12	1.83E-12	1.83E-12	6.84E-13	6.84E-13
	9	1.83E-12	1.83E-12	1.83E-12	1.83E-12	5.22E-12	5.22E-12
	10	2.20E-12	2.20E-12	2.20E-12	2.20E-12	2.18E-12	2.04E-12
1E-12	**1**	3.09E-14	2.68E-14	4.23E-14	1.93E-15	3.11E-15	4.57E-15
	2	2.20E-15	1.83E-15	1.47E-15	1.90E-15	7.57E-15	6.94E-15
	3	2.68E-14	7.88E-14	6.92E-13	3.11E-15	3.53E-15	3.99E-15
	4	6.99E-14	5.97E-15	9.89E-15	4.90E-14	3.00E-15	1.54E-14
	5	3.31E-15	1.54E-15	9.47E-16	7.47E-15	8.61E-16	6.24E-16
	6	2.14E-15	1.52E-14	1.72E-13	2.85E-15	1.29E-15	1.12E-14
	7	2.31E-14	2.31E-14	2.31E-14	2.31E-14	1.97E-14	1.97E-14
	8	1.83E-15	1.83E-15	1.83E-15	1.83E-15	6.84E-16	6.84E-16
	9	1.83E-15	1.83E-15	1.83E-15	1.83E-15	5.22E-15	5.22E-15
	10	2.20E-15	2.20E-15	2.20E-15	2.20E-15	2.18E-15	2.04E-15

Table 6: The Analysis of ODEs for convergence limits of SiO_2/H_2O and $MoS_2 - Sio_2/H_2O$

Convergence Limit	Scenarios	SiO_2/H_2O			$MoS_2 - SiO_2/H_2O$		
		Case-1	**Case-2**	**Case-3**	**Case-1**	**Case-2**	**Case-3**
1E-09	**1**	45603	42814	45602	44548	44752	46945
	2	47470	49000	49000	49017	41970	41970
	3	42814	41855	46503	44752	43647	47030
	4	44928	47946	44599	41630	45193	37400
	5	45251	47028	44699	41953	45090	43764
	6	46816	43893	47906	43092	45423	45415
	7	43024	43024	43024	43024	39035	39035
	8	49000	49000	49000	49000	44223	44223
	9	49000	49000	49000	49000	47742	47742
	10	47470	47470	47470	47470	46722	45702
1E-12	**1**	45603	42814	45602	44548	44752	46945
	2	47470	49000	49000	49017	41970	41970
	3	42814	44396	46503	44752	43647	47030
	4	44928	47946	44599	41630	45193	39907
	5	45251	47028	44699	41953	45090	43764
	6	46816	46546	47906	43092	45423	45415
	7	43024	43024	43024	43024	41760	41760
	8	49000	49000	49000	49000	44223	44223
	9	49000	49000	49000	49000	47742	47742
	10	47470	47470	47470	47470	46722	45702

Table 7: The Numerical data analysis of Skin friction for SiO_2/H_2O and $MoS_2 - Sio_2/H_2O$

Parameter	SiO_2/H_2O			$MoS_2 - SiO_2/H_2O$		
	$m = 3.7$	$m = 5.9$	$m = 7.9$	$m = 3.7$	$m = 5.9$	$m = 7.9$
ϕ_1/ϕ_2	0.2131	0.2020	0.1920	0.3271	0.3112	0.2970
λ	0.4182	0.4062	0.3902	0.4314	0.4452	0.4488
M	0.2020	0.1876	0.1745	0.3112	0.2854	0.2616
E	0.3548	0.3708	0.3913	0.4634	0.4927	0.5337
N	0.3380	0.4303	0.4892	0.4500	0.5468	0.6078
S	0.4182	0.4182	0.4182	0.4182	0.4975	0.5067

Table 8: The Numerical data analysis of local Nusselt number for SiO_2/H_2O and $MoS_2 - Sio_2/H_2O$

Parameter	SiO_2/H_2O			$MoS_2 - SiO_2/H_2O$		
	$m = 3.7$	$m = 5.9$	$m = 7.9$	$m = 3.7$	$m = 5.9$	$m = 7.9$
ϕ_1/ϕ_2	3.6801	3.6062	3.5322	3.5336	3.4633	3.3963
λ	9.9452	10.6115	11.2739	6.4196	6.8556	7.2842
M	10.6115	10.6010	10.5918	6.8556	6.8331	6.8127
E	4.6754	4.0080	3.1504	3.4374	2.5739	1.3459
N	4.9096	3.2791	2.5856	3.4245	2.3957	1.9432
S	4.9258	8.6943	12.8249	3.6603	5.9823	8.6339

Table 9: The Analysis of BCs for convergence limits of SiO_2/H_2O and $MoS_2 - Sio_2/H_2O$

Convergence Limit	Scenarios	SiO_2/H_2O			$MoS_2 - SiO_2/H_2O$		
		Case-1	Case-2	Case-3	Case-1	Case-2	Case-3
1E-09	1	95	78	78	78	78	78
	2	78	78	78	78	94	94
	3	/78	94	95	78	78	78
	4	94	78	78	94	78	77
	5	94	78	78	94	78	78
	6	96	95	96	94	94	78
	7	94	94	94	94	77	77
	8	78	78	78	78	78	78
	9	78	78	78	78	95	95
	10	78	78	78	78	78	78
1E-12	1	95	78	78	78	78	78
	2	78	78	78	78	94	94
	3	78	95	95	78	78	78
	4	94	78	78	94	78	78
	5	94	78	78	94	78	78
	6	96	96	96	94	94	78
	7	94	94	94	94	78	78
	8	78	78	78	78	78	78
	9	78	78	78	78	95	95
	10	78	78	78	78	78	78

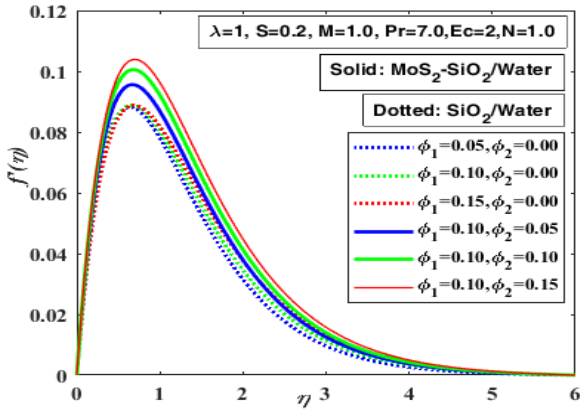

Figure 7: Impact of ϕ_1 and ϕ_2 on $f'(\eta)$

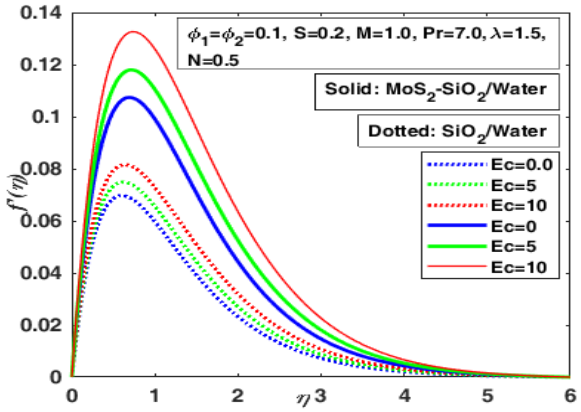

Figure 8: The effect of Eckert number (Ec) on $f'(\eta)$

the injection case and when $S < 0$, it presents the suction case. Moreover, the value of $f'(\eta)$, almost reaches 0.1 for $S = 0.2$ which is far greater than the value of $f'(\eta)$ for SiO_2/H_2O at the same value of S. This figure clearly shows that as S is increased, the velocity reduces as a result of the surface suction acting in opposition to the flow of fluid, which results in a reduction in velocity. Additionally, nanofluid exhibits a far greater velocity decrease than hybrid nanofluid. It is notable that this difference is more significant as compared to other values of S. Furthermore, decreased NF velocity is significantly greater than the HNF. The influence of the volumetric fraction of both NFs is examined by Fig7. It is shown that the velocity of fluid grows with the change in all volumetric fractions of NPs.

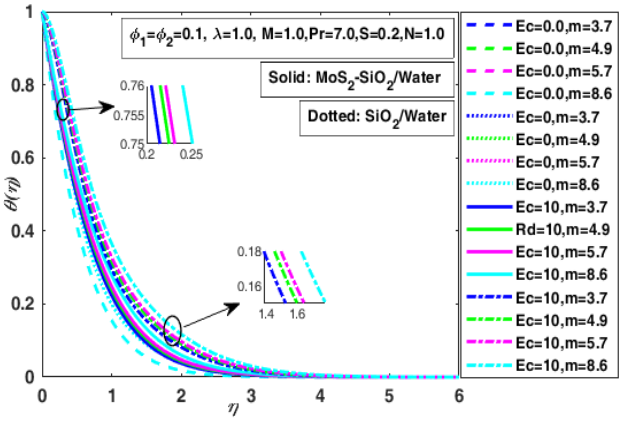

Figure 9: Impact of Eckert number (Ec) on $\theta(\eta)$

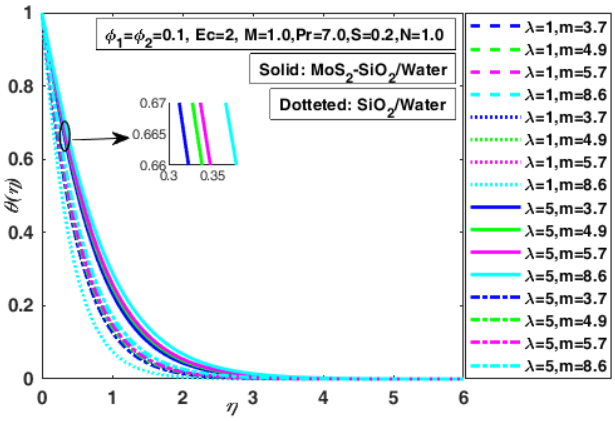

Figure 10: Impact of Power index (λ) on $\theta(\eta)$

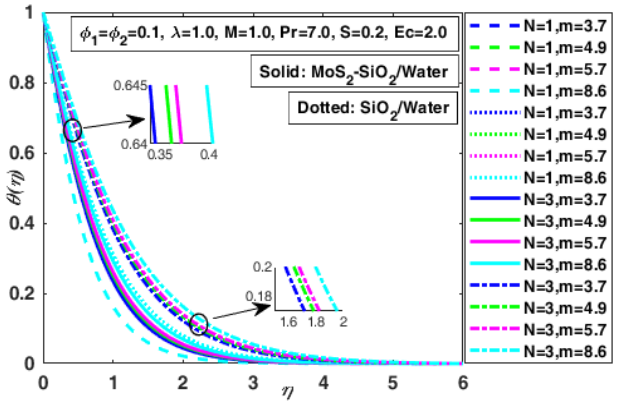

Figure 11: Impact of radiation parameter (N) on $\theta(\eta)$

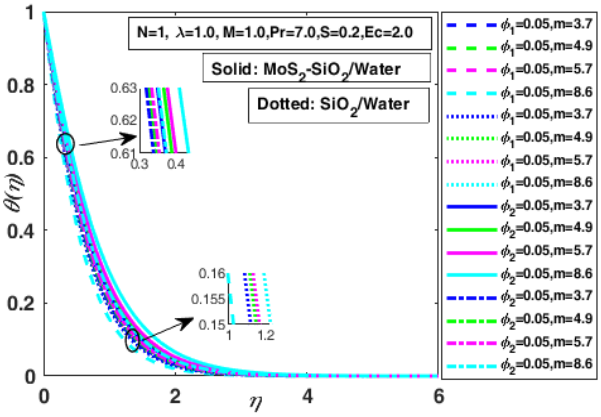

Figure 12: The impact of ϕ_1 and ϕ_2 on $\theta(\eta)$

The SiO_2 volumetric-fraction of HNF has been settled at 1%. The increasing trend in fluid velocity is related to the point that HNF and NF dynamic viscosity is in inverse relation to volumetric fractions of nano-particles. As a result, the increase in ϕ_1 and ϕ_2 means a reduction in the base fluid viscosity and this accelerates the fluid flow. Furthermore, the fluid velocity is observed more in the case of the HNF. Eckert number Ec influences are indicated in Fig8. It can be seen from this figure that the increased Eckert number leads to the acceleration of both forms of NF flow. Moreover, in the case of HNF, this change is considerably greater. Fig9 considering four different values of the nano-particles shaping factors for NF and also HNFS is arranged for various values of Eckert number. From such a figure it has been shown that the distribution of temperatures in both forms of NFs increases with the Eckert number. Fig10 and Fig11 are plotted for increasing values of power law index λ and N (thermal radiation parameter) respectively.

From these graphical figures, it is also noted that the distributions of NF and HNF temperatures rise via an increase for both N and λ. The influence of volumetric fractions of the nano-particles is shown in Fig12. It is noticed that throughout the presence of NF and HNF, the rise in volumetric fractions ϕ_1 and ϕ_2 contributes to increased temperature, respectively.

Table 7 reported the computed values of the Nusselt number in tabular form. The local Nusselt number upgraded by raising λ, Qh, We, Pr and Bi while decay by increments in M^*, ϕ_w, δ, Sc, K_1, Nr, Nt, A^*, α and β^*. The computed numerical data of Skin friction is rendered in Table 8. The Skin friction grows for the magnetic parameter, Schmidt, and local Weisenberge number while declines for the temperature ratio parameter, unsteadiness, and shear rate parameter respectively. The complexity of the proposed computational approach is interpreted in terms of tabulated data for each fluidic parameter. The mesh points analysis of the considered fluidic model acquired by the proposed numerical approach is tabulated in Table 4 while Table 5 depicted the computed values of residual error by Lobatto IIIA approach for each sundry physical fluidic parameter. The computed numerical data of ODEs for involved sundry parameters attained by the proposed scheme are illustrated in Table 6 while the computed numerical data of BCs for emerging physical parameters are tabulated in Table 9.

4. Conclusion, novelty and recommendations

This article portrays a numerical investigation of porous surfaces for convection. The nano-fluidic model is based on the inverted cone along with porous boundary for both NF $SiO_2/water$ and HNF $MoS_2 - SiO_2/water$ respectively. We observed that fluid velocity reduces with a rise in λ and as compared to HNF. The decrease in the flow of fluid is greater in the case of NF. It is also observed that the flow of fluid for $SiO_2/water$ NF decelerates more as compared to the HNF.

The fluid flow decelerates as λ increases, and NFs shows the deceleration more pronouncedly than HNFs. With a rise in $S > 0$, velocity decreases. Moreover, it has been observed that fluidic flow slows down more for $SiO_2/water$ NF than for HNF. Both forms of NF flow are accelerated by a rise in Eckert number. In

the case of HNF, this rise is also much greater. The momentum and fluid flow boundary layer thickness of NF and HNFs are accelerated by a rise in the heat radiation parameter N. For both NF and HNFs, the skin friction coefficient and Nusselt number rise as the volumetric fractions of nanoparticles increase by ϕ_1 and ϕ_2, respectively.

A HNF with blade-shaped nanoparticles also exhibits the highest skin friction coefficient and Nusselt number, whereas brick-shaped nanoparticles suspended in a NF exhibit the lowest. In the case of $SiO_2/water$ NF, skin friction coefficient rises with an increase in suction parameter S, however the opposite trend is observed for $MoS_2 - SiO_2/water$ HNF. Brick shape nanoparticles hanged in $SiO_2/water$ NF exhibit the lowest magnitude, and blade shape nanoparticles hanged in $MoS_2 - SiO_2/water$ HNF exhibit the highest magnitude. For both NF and HNFs, the Nusselt number rises with increasing the suction parameter values. As viscous dissipation and harmful radiation increase, skin friction coefficient rises and Nusselt's number falls. Exhaustive analysis of these statistics shows that the HNF plays a significant role in transport of fluids and an elevated temperature distribution for NF is achieved.

The various characteristics of the 3-D MHD flow of HNF with thermal (heat) radiation features can be explored, in the future by novel and advanced artificial intelligence-based numerical computation skills, see for example [40], [41], [42], [43], [44].

5. Statements & Declarations

5.1. Funding

The authors affirm that they did not accept any funding, incentives, or other assistance for the preparation of this article.

5.2. Competing Interests

There are no significant financial or non-financial objectives of the authors to disclose.

5.3. Data Availability

The datasets created for and/or used in the analysis of the current research are accessible upon request.

References

[1] C. Ouyang, R. Akhtar, M. A. Z. Raja, M. Touseef Sabir, M. Awais, M. Shoaib, Numerical treatment with lobatto iiia technique for radiative flow of mhd hybrid nanofluid (al2o3cu/h2o) over a convectively heated stretchable rotating disk with velocity slip effects, AIP Advances 10 (5) (2020) 055122.

[2] K. Ahmadi, S. Khanmohammadi, S. Khanmohammadi, M. Bahiraei, Q.-V. Bach, Heat transfer assessment of turbulent nanofluid flow in a circular pipe fitted with elliptical-cut twisted tape inserts, Journal of Thermal Analysis and Calorimetry (2020) 1–14.

[3] V. Narla, D. Tripathi, O. A. Bég, Analysis of entropy generation in biomimetic electroosmotic nanofluid pumping through a curved channel with joule dissipation, Thermal Science and Engineering Progress 15 (2020) 100424.

[4] E. Maraj, Z. Iqbal, E. Azhar, Z. Mehmood, A comprehensive shape factor analysis using transportation of mos2-sio2/h2o inside an isothermal semi vertical inverted cone with porous boundary, Results in physics 8 (2018) 633–641.

[5] M. Ali, M. F. Sahito, N. K. Jha, S. Memon, A. Keshavarz, S. Iglauer, A. Saeedi, M. Sarmadivaleh, et al., Effect of nanofluid on co2-wettability reversal of sandstone formation; implications for co2 geo-storage, Journal of colloid and interface science 559 (2020) 304–312.

[6] I. Ahmad, T. N. Cheema, M. A. Z. Raja, S. E. Awan, N. B. Alias, S. Iqbal, M. Shoaib, A novel application of lobatto iiia solver for numerical treatment of mixed convection nanofluidic model, Scientific Reports 11 (1) (2021) 1–16.

[7] M. Shoaib, M. A. Z. Raja, M. T. Sabir, M. Awais, S. Islam, Z. Shah, P. Kumam, Numerical analysis of 3-d mhd hybrid nanofluid over a rotational disk in presence of thermal radiation with joule heating and viscous dissipation effects using lobatto iiia technique, Alexandria Engineering Journal 60 (4) (2021) 3605–3619.

[8] S. Ali, M. A. Z. Raja, T. N. Cheema, I. Ahmad, N. Mian, M. Shoaib, Analysis of williamson nanofluid with velocity and thermal slips past over a stretching sheet by lobatto iiia numerically, Thermal Science (00) (2021) 159–159.

[9] S. Choi, D. Singer, H. Wang, et al., Developments and applications of non-newtonian flows, Asme Fed 66 (1995) 99–105.

[10] W. Khan, I. Pop, Boundary-layer flow of a nanofluid past a stretching sheet, International journal of heat and mass transfer 53 (11-12) (2010) 2477–2483.

[11] R. S. R. Gorla, A. Chamkha, Natural convective boundary layer flow over a nonisothermal vertical plate embedded in a porous medium saturated with a nanofluid, Nanoscale and Microscale Thermophysical Engineering 15 (2) (2011) 81–94.

[12] B. Gireesha, B. Mahanthesh, R. S. R. Gorla, Suspended particle effect on nanofluid boundary layer flow past a stretching surface, Journal of nanofluids 3 (3) (2014) 267–277.

[13]

[14] T.-Y. Na, J. Chiou, Laminar natural convection over a frustum of a cone, Applied Scientific Research 35 (5-6) (1979) 409–421.

[15] K. Yih, Coupled heat and mass transfer by free convection over a truncated cone in porous media: Vwt/vwc or vhf/vmf, Acta Mechanica 137 (1-2) (1999) 83–97.

[16] A. J. Chamkha, Coupled heat and mass transfer by natural convection about a truncated cone in the presence of magnetic field and radiation effects, Numerical Heat Transfer: Part A: Applications 39 (5) (2001) 511–530.

[17] D. Nield, A. Kuznetsov, The cheng–minkowycz problem for natural convective boundary-layer flow in a porous medium saturated by a nanofluid, International Journal of Heat and Mass Transfer 52 (25-26) (2009) 5792–5795.

[18] A. Kuznetsov, D. Nield, Natural convective boundary-layer flow of a nanofluid past a vertical plate, International Journal of Thermal Sciences 49 (2) (2010) 243–247.

[19]

[20]

[21]

[22] I. Ahmad, S. I. Hussain, M. Usman, H. Ilyas, On the solution of zabolotskaya–khokhlov and diffusion of oxygen equations using a sinc collocation method, Partial Differential Equations in Applied Mathematics 4 (2021) 100066.

[23] I. Ahmad, S. I. Hussain, H. Ilyas, J. L. García Guirao, A. Ahmed, S. Rehmat, T. Saeed, Numerical solutions of schrödinger wave equation and transport equation through sinc collocation method, Nonlinear Dynamics 105 (1) (2021) 691–705.

[24] I. Ahmad, S.-u.-I. Ahmad, K. Kutlu, H. Ilyas, S. I. Hussain, F. Rasool, On the dynamical behavior of nonlinear fitzhugh–nagumo and bateman–burger equations in quantum model using sinc collocation scheme, The European Physical Journal Plus 136 (11) (2021) 1–24.

[25] I. Ahmad, H. Ilyas, K. Kutlu, V. Anam, S. I. Hussain, J. L. G. Guirao, Numerical computing approach for solving hunter-saxton equation arising in liquid crystal model through sinc collocation method, Heliyon 7 (7) (2021) e07600.

[26] A. Noghrehabadi, A. Behseresht, M. Ghalambaz, Natural convection of nanofluid over vertical plate embedded in porous medium: prescribed surface heat flux, Applied mathematics and mechanics 34 (6) (2013) 669–686.

[27] A. Zeeshan, R. Ellahi, M. Hassan, Magnetohydrodynamic flow of water/ethylene glycol based nanofluids with natural convection through a

porous medium, The European Physical Journal Plus 129 (12) (2014) 261.
[28] R. Ellahi, M. Hassan, A. Zeeshan, Shape effects of nanosize particles in cu–h2o nanofluid on entropy generation, International Journal of Heat and Mass Transfer 81 (2015) 449–456.
[29] P. K. Namburu, D. P. Kulkarni, D. Misra, D. K. Das, Viscosity of copper oxide nanoparticles dispersed in ethylene glycol and water mixture, Experimental Thermal and Fluid Science 32 (2) (2007) 397–402.
[30] H. Chen, Y. Ding, C. Tan, Rheological behaviour of nanofluids, New journal of physics 9 (10) (2007) 367.
[31] H. Chen, Y. Ding, A. Lapkin, Rheological behaviour of nanofluids containing tube/rod-like nanoparticles, Powder Technology 194 (1-2) (2009) 132–141.
[32] N. Masoumi, N. Sohrabi, A. Behzadmehr, A new model for calculating the effective viscosity of nanofluids, Journal of Physics D: Applied Physics 42 (5) (2009) 055501.
[33] A. Afshari, M. Akbari, D. Toghraie, M. E. Yazdi, Experimental investigation of rheological behavior of the hybrid nanofluid of mwcnt–alumina/water (80%)–ethylene-glycol (20%), Journal of Thermal Analysis and Calorimetry 132 (2) (2018) 1001–1015.
[34] H. U. Kang, S. H. Kim, J. M. Oh, Estimation of thermal conductivity of nanofluid using experimental effective particle volume, Experimental Heat Transfer 19 (3) (2006) 181–191.
[35] A. H. Nagoor, E. S. Alaidarous, M. T. Sabir, M. Shoaib, M. A. Z. Raja, Numerical treatment for three-dimensional rotating flow of carbon nanotubes with darcy–forchheimer medium by the lobatto iiia technique, AIP Advances 10 (2) (2020) 025016.
[36] I. Uddin, R. Akhtar, Z. Zhiyu, S. Islam, M. Shoaib, M. A. Z. Raja, Numerical treatment for darcy-forchheimer flow of sisko nanomaterial with nonlinear thermal radiation by lobatto iiia technique, Mathematical Problems in Engineering 2019.
[37] I. Uddin, R. Akhtar, M. A. R. Khan, Z. Zhiyu, S. Islam, M. Shoaib, M. A. Z. Raja, Numerical treatment for fluidic system of activation energy with non-linear mixed convective and radiative flow of magneto nanomaterials with naviers velocity slip, AIP Advances 9 (5) (2019) 055210.
[38] C. Ouyang, R. Akhtar, M. A. Z. Raja, M. Touseef Sabir, M. Awais, M. Shoaib, Numerical treatment with lobatto iiia technique for radiative flow of mhd hybrid nanofluid (al2o3cu/h2o) over a convectively heated stretchable rotating disk with velocity slip effects, AIP Advances 10 (5) (2020) 055122.
[39] T.-C. Sun, I. Uddin, M. A. Z. Raja, M. Shoaib, I. Ullah, W. Jamshed, S. Islam, Numerical investigation of thin-film flow over a rotating disk subject to the heat source and nonlinear radiation: Lobatto iiia approach, Waves in Random and Complex Media (2022) 1–15.
[40] Z. Sabir, M. A. Z. Raja, M. Umar, M. Shoaib, Design of neuro-swarming-based heuristics to solve the third-order nonlinear multi-singular emden–fowler equation, The European Physical Journal Plus 135 (6) (2020) 1–17.
[41] F. Faisal, M. Shoaib, M. A. Z. Raja, et al., A new heuristic computational solver for nonlinear singular thomas–fermi system using evolutionary optimized cubic splines, The European Physical Journal Plus 135 (1) (2020) 1–29.
[42] I. Ahmad, H. Ilyas, A. Urooj, M. S. Aslam, M. Shoaib, M. A. Z. Raja, Novel applications of intelligent computing paradigms for the analysis of nonlinear reactive transport model of the fluid in soft tissues and microvessels, Neural Computing and Applications 31 (12) (2019) 9041–9059.
[43] A. H. Bukhari, M. Sulaiman, S. Islam, M. Shoaib, P. Kumam, M. A. Z. Raja, Neuro-fuzzy modeling and prediction of summer precipitation with application to different meteorological stations, Alexandria Engineering Journal 59 (1) (2020) 101–116.
[44] T. N. Cheema, M. A. Z. Raja, I. Ahmad, S. Naz, H. Ilyas, M. Shoaib, Intelligent computing with levenberg–marquardt artificial neural networks for nonlinear system of covid-19 epidemic model for future generation disease control, The European Physical Journal Plus 135 (11) (2020) 1–35.